



## Fire-Induced Thermal Fields in Window Glass. I—Theory

A. A. Joshi\* & P. J. Pagni

Mechanical Engineering Department, University of California at Berkeley, Berkeley,  
California 94720, USA

(Received 5 November 1992; revised version received 21 April 1993;  
accepted 10 May 1993)

### ABSTRACT

*Window glass breaking plays an important role in compartment fire dynamics as the window acts as a wall before breaking and as a vent after breaking. Previous work suggested a model for the time to breakage of a window glass exposed to a particular fire. In this paper, the glass thermal fields obtained using that model are examined in detail. The temperature field dependence on heat transfer coefficients, radiative decay length and flame radiation is explored. The results show that the glass surface temperature increases with a decrease in the decay length and increases with an increase in flame radiation heat flux. Early in the fire, the glass temperature may be higher than the hot layer temperature due to direct impingement of flame radiation. Later the glass temperature lags the hot layer temperature. The variation of the time to breakage as a function of the shading width and decay length is also presented and the results indicate that the breaking time decreases with an increase in the shading width and decreases with a decrease in decay length. Heat flux maps for typical conditions indicate that most of the heat influx is stored in the glass, increasing its temperature.*

### NOTATION

<i>A–G</i>	Constants
<i>Bi</i>	Biot number, $hL/k$
<i>c</i>	Specific heat capacity

\* Present address: Mechanical Engineering Department, University of California, Santa Barbara, California 93106, USA.

$E$	Young's modulus
$F$	Kernels
$h$	Heat transfer coefficient
$H$	half-width of the window
$I$	Radiant heat flux directly from the flame
$j(t)$	$= I(t)L/kT_c$ , see eqn (6)
$k$	Thermal conductivity
$l$	Decay length
$L$	Glass thickness
$q$	Dimensional heat flux
$Q$	Energy
$s$	Shaded length
$T$	Temperature
$u$	Dummy variable

*Greek*

$\alpha$	Thermal diffusivity
$\beta$	Thermal expansion coefficient
$\gamma$	Dimensionless decay length, $l/L$
$\varepsilon$	Emissivity
$\theta$	Dimensionless temperature
$\xi$	Dimensionless $x$ coordinate
$\sigma$	Stress
$\tau$	Dimensionless time
$\phi$	Dimensionless heat flux

*Subscripts*

1	Ambient (outside) side of glass pane
2	Compartment side of glass pane
b	Breakage
c	Characteristic, convection
f	Flame radiation
i	Initial
r	Radiation
s	Stored in glass
y	Diffusion in shaded portion
$\infty$	Ambient

## INTRODUCTION

Window glass breaking in fires is an important practical problem, since a window acts as a wall before breaking and as a vent after breaking. Thus, the knowledge of the time to window breakage is crucial in order

to predict the evolving compartment fire dynamics. Emmons<sup>1</sup> highlighted the importance of glass breaking in fires, and, based on Harvard experiments,<sup>2</sup> suggested thermally induced tensile stresses as the mechanism for glass breakage. All window glass has its surrounding edge covered by an opaque frame or gasket. Glass is a relatively poor thermal conductor. The central portion of the window is heated by infrared radiation and hot gas convection, while the frame protects the shaded edge so that it remains near its initial temperature. The thermal expansion of the central portion places the covered edge in tension until it cracks. These cracks then bifurcate and quickly propagate, causing the window to become a vent. This scenario suggests a simple criterion<sup>3</sup> for the temperature rise required to break glass windows in fires which follows directly from Hooke's law:<sup>4</sup>

$$\beta \Delta T = \sigma_b / E \quad (1)$$

where  $\Delta T$  is the temperature difference between the glass edge and center;  $\beta$  is the thermal coefficient of linear expansion;  $\sigma_b$  is the breaking stress; and  $E$  is the Young's modulus for glass. Keski-Rahkonen did excellent analyses<sup>5,6</sup> of the limiting cases where: (1) there are no temperature gradients across the glass thickness so a constant heat input can be treated as a volumetric heat source; (2) convective and linearized radiative heat losses are constant and identical on both sides of the glass so it can also be treated as a volumetric heat sink; and (3) all gas temperatures, the initial temperature and the temperature of the outer edge are constant and identical. His analytic results confirm eqn (1) as a lower limit for  $\Delta T$ . While the restrictions make it difficult to apply these analyses directly to compartment fires, they do describe small-scale experiments with large, constant radiative heat influx.<sup>2</sup>

Skelly *et al.*<sup>7</sup> did an experimental study of glass breaking in compartment fires. They burned liquid fuel in pans inside a compartment which had a glass window and recorded the temperature histories of the glass and hot gas layer inside the compartment. This experimental study also indicates that eqn (1) is a reasonable first approximation for the glass temperature at breakage. What remains is to model energy transfer between the fire, the window glass and the ambience, in order to predict the time at which the glass breakage temperature is reached. Techniques to calculate accurately the history of the central glass temperature profile,  $T(x, t)$ , by taking the Laplace transform of the temperature and numerically integrating the resulting equations, have been described.<sup>8</sup> Two-dimensional temperature histories,  $T(x, y, t)$ , and mean stress histories,  $\sigma_{zz}(y, t)$ , were also presented.

This paper examines in detail the thermal fields obtained from that

model.<sup>8</sup> The following problems are addressed: (1) the nature of kernels arising from Laplace transform of the temperature; (2) parameter effects on the temperature profiles within the glass thickness; (3) the dependence of the temperature histories of the central exposed glass surfaces on the Biot number, the dimensionless decay length,  $\gamma$ , and the unsteady dimensionless incident radiative flux,  $j(\tau)$ ; and (4) the dependence of the dimensionless breaking time,  $\tau_b$ , on the dimensionless shading width,  $s/L$ . The dependence on the heat transfer coefficient at the outer surface is not explored because it is not expected to vary significantly in a fire environment.

### THEORY

Consider the window shown in Fig. 1. For large shading,  $s/L \geq 2$ , and fast heating,  $\alpha t_b/s^2 \leq 1$ , where  $s$  is the width of the shading and  $L$  is the glass thickness, the temperature difference  $\Delta T$  in eqn (1) corresponds to the temperature difference between the initial temperature of the unheated outer edge and the transient temperature of the uniformly heated central section of the glass.<sup>8</sup> The goal then is to determine the temperature in the large central section of the glass as a function of depth into the glass,  $x$ , and time,  $t$ . Significant temperature gradients,  $\partial T/\partial x$  were shown to exist since the heat source is on the inside of the window and the sink is on the outside. The unshaded glass is uniformly

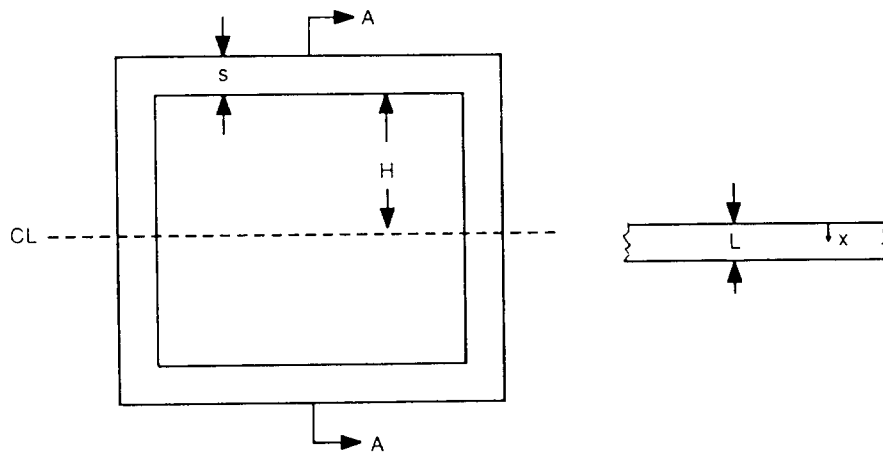


Fig. 1. Window geometry showing the coordinate,  $x$ , and length parameters.  $x$ , Depth into the window;  $s$ , width of the shading;  $H$ , half-height;  $L$ , glass thickness.

heated, so  $\partial/\partial y$  and  $\partial/\partial z$  are zero. The governing equation is:

$$\rho c \frac{\partial T}{\partial t} = k \frac{\partial^2 T}{\partial x^2} + I(t) \frac{e^{-x/l}}{l} \quad (2)$$

where  $I(t)$  is the incident radiative flux directly from the fire which is at sufficiently short wavelengths that its distributed internal absorption needs to be included,<sup>9</sup> and  $l$  is the decay length in the glass. With the assumption that the glass is grey to other radiation, the initial and boundary conditions are:

$$\text{at } t = 0, \quad T = T_i, \quad (3)$$

$$\text{at } x = 0, \quad -k \frac{\partial T}{\partial x} = h_2(T_{2\infty}(t) - T(0, t)) + \varepsilon_{2\infty} \sigma T_{2\infty}^4(t) - \varepsilon \sigma T^4(0, t) = q_2(t) \quad (4)$$

$$\text{at } x = L, \quad -k \frac{\partial T}{\partial x} = h_1(T(L, t) - T_{1\infty}(t)) + \varepsilon \sigma T^4(L, t) - \varepsilon_{1\infty} \sigma T_{1\infty}^4(t) = q_1(t) \quad (5)$$

where side 1 is toward outside ambience and side 2 is toward the hot layer inside the compartment.

With the definitions:

$$\xi = \frac{x}{L}; \quad \tau = \frac{\alpha t}{L^2}; \quad \gamma = \frac{l}{L}; \quad \theta = \frac{T - T_i}{T_c};$$

$$T_c = \sigma_b / E\beta - T_i; \quad \phi_1 = \frac{q_1}{kT_c/L}; \quad \phi_2 = \frac{q_2}{kT_c/L}; \quad j(\tau) = \frac{I(t)}{kT_c/L} \quad (6)$$

the dimensionless governing equation is:

$$\frac{\partial \theta}{\partial \tau} = \frac{\partial^2 \theta}{\partial \xi^2} + j(\tau) \frac{e^{-\xi/\gamma}}{\gamma} \quad (7)$$

with dimensionless initial and boundary conditions:

$$\text{at } \tau = 0, \quad \theta = 0, \quad (8)$$

$$\text{at } \xi = 0, \quad -\frac{\partial \theta}{\partial \xi} = \phi_2(\tau), \quad (9)$$

$$\text{at } \xi = 1, \quad -\frac{\partial \theta}{\partial \xi} = \phi_1(\tau). \quad (10)$$

Explicit expressions for the dimensionless heat fluxes,  $\phi_1(\tau)$  and  $\phi_2(\tau)$ ,

are given in the Appendix. This equation is solved using a Laplace transform on time:

$$\theta^* = \int_0^\infty \theta e^{-\nu\tau} d\tau \quad (11)$$

The solution for both surface temperatures is given by:

$$\begin{aligned} \theta(0, \tau) = & 2 \int_0^{\sqrt{\tau}} F_1(0, u) \phi_1(\tau - u^2) du + 2 \int_0^{\sqrt{\tau}} F_2(0, u) \phi_2(\tau - u^2) du \\ & + \frac{2}{\gamma} \int_0^{\sqrt{\tau}} F_3(0, u) j(\tau - u^2) du \quad (12) \end{aligned}$$

and:

$$\begin{aligned} \theta(1, \tau) = & 2 \int_0^{\sqrt{\tau}} F_1(1, u) \phi_1(\tau - u^2) du + 2 \int_0^{\sqrt{\tau}} F_2(1, u) \phi_2(\tau - u^2) du \\ & + \frac{2}{\gamma} \int_0^{\sqrt{\tau}} F_3(1, u) j(\tau - u^2) du \quad (13) \end{aligned}$$

where the  $F_i(\xi, u)$  are kernels which are functions of  $\gamma$ ,  $\xi$  and  $u$  and are for short time,  $u < 0.4$ :

$$F_1(\xi, u) = -\frac{1}{\sqrt{\pi}} \left[ \sum_{k=0}^{\infty} e^{-(\xi-2k-1)^2/4u^2} + \sum_{k=0}^{\infty} e^{-(\xi+2k+1)^2/4u^2} \right] \quad (14)$$

$$F_2(\xi, u) = \frac{1}{\sqrt{\pi}} \left[ \sum_{k=0}^{\infty} e^{-(\xi+2k)^2/4u^2} + \sum_{k=1}^{\infty} e^{-(\xi-2k)^2/4u^2} \right] \quad (15)$$

and:

$$\begin{aligned} F_3(\xi, u) = & u \left[ e^{-\xi/\gamma} e^{u^2/\gamma^2} \right. \\ & + \frac{1}{2} e^{-\xi/\gamma} e^{u^2/\gamma^2} \left[ \sum_{k=0}^{\infty} \operatorname{erfc} \left( \frac{2k+1-\xi}{\sqrt{4u^2}} - \sqrt{\frac{u^2}{\gamma^2}} \right) e^{-(2k+1-\xi)/\gamma} \right. \\ & \left. - \operatorname{erfc} \left( \frac{2k+1-\xi}{\sqrt{4u^2}} + \sqrt{\frac{u^2}{\gamma^2}} \right) e^{(2k+1-\xi)/\gamma} \right. \\ & \left. + \sum_{k=0}^{\infty} \operatorname{erfc} \left( \frac{2k+1+\xi}{\sqrt{4u^2}} - \sqrt{\frac{u^2}{\gamma^2}} \right) e^{-(2k+1+\xi)/\gamma} \right. \end{aligned}$$

$$\begin{aligned}
& - \operatorname{erfc} \left( \frac{2k+1+\xi}{\sqrt{4u^2}} + \sqrt{\frac{u^2}{\gamma^2}} \right) e^{(2k+1+\xi)/\gamma} \Big] \\
& - \frac{1}{2} e^{u^2/\gamma} \left[ \sum_{k=0}^{\infty} \operatorname{erfc} \left( \frac{2k+\xi}{\sqrt{4u^2}} - \sqrt{\frac{u^2}{\gamma^2}} \right) e^{-(2k+\xi)/\gamma} \right. \\
& - \operatorname{erfc} \left( \frac{2k+\xi}{\sqrt{4u^2}} + \sqrt{\frac{u^2}{\gamma^2}} \right) e^{(2k+\xi)/\gamma} \\
& + \sum_{k=1}^{\infty} \operatorname{erfc} \left( \frac{2k-\xi}{\sqrt{4u^2}} - \sqrt{\frac{u^2}{\gamma^2}} \right) e^{-(2k-\xi)/\gamma} \\
& \left. - \operatorname{erfc} \left( \frac{2k-\xi}{\sqrt{4u^2}} + \sqrt{\frac{u^2}{\gamma^2}} \right) e^{(2k-\xi)/\gamma} \right] \quad (16)
\end{aligned}$$

and for long time,  $u > 0.4$ :

$$F_1(\xi, u) = -u \left( 1 + 2 \sum_{k=1}^{\infty} (-1)^k \cos(k\pi\xi) e^{-k^2\pi^2 u^2} \right) \quad (17)$$

$$F_2(\xi, u) = u \left( 1 + 2 \sum_{k=1}^{\infty} (-1)^k \cos(k\pi(1-\xi)) e^{-k^2\pi^2 u^2} \right) \quad (18)$$

and;

$$\begin{aligned}
F_3(\xi, u) = u \left[ e^{-1/\gamma} \left[ -\gamma + \frac{2}{\gamma} \sum_{k=1}^{\infty} \frac{(-1)^k \cos(k\pi\xi)}{-k^2\pi^2 - (1/\gamma^2)} e^{-k^2\pi^2 u^2} \right] \right. \\
\left. - \left[ -\gamma + \frac{2}{\gamma} \sum_{k=1}^{\infty} \frac{(-1)^k \cos(k\pi(1-\xi))}{-k^2\pi^2 - (1/\gamma^2)} e^{-k^2\pi^2 u^2} \right] \right] \quad (19)
\end{aligned}$$

The numerical procedure was the trapezoidal rule with constant time steps and thus variable  $\Delta u$ , since the  $\phi_i$  are functions of  $\theta$  which is known only at each time step. Newton-Raphson's method for finding roots of non-linear equations was also utilized.

## KERNELS

Figure 2a shows the variation of  $F_1(0, u)$  and  $F_2(0, u)$  with  $u$ . From eqn (12) it is evident that the area under the curve  $F_1(0, u)$  from  $u = 0$  to  $\sqrt{\tau}$  is equal to the temperature of the inner surface  $\theta(0, \tau)$  for  $\phi_1 = \frac{1}{2}$  with

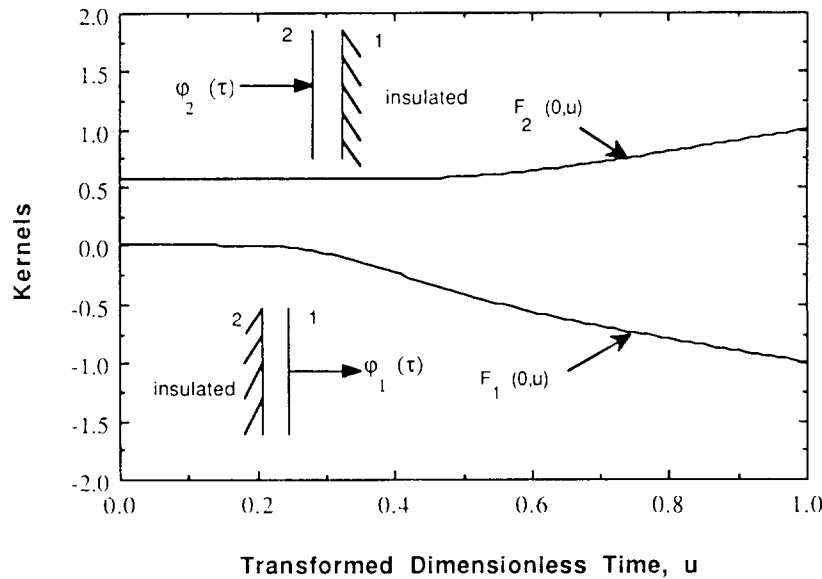


**Fig. 2a.** Variation of kernels  $F_1(0, u)$  and  $F_2(0, u)$ . The area under the curve  $F_1(0, u)$  from 0 to  $\sqrt{\tau}$  is the temperature of the inner surface for the sample case,  $\phi_1 = \frac{1}{2}$  and  $j = \phi_2 = 0$ . The area under the curve  $F_2(0, u)$  from 0 to  $\sqrt{\tau}$  is the temperature of the inner surface for the sample case,  $\phi_2 = \frac{1}{2}$  and  $j = \phi_1 = 0$ .

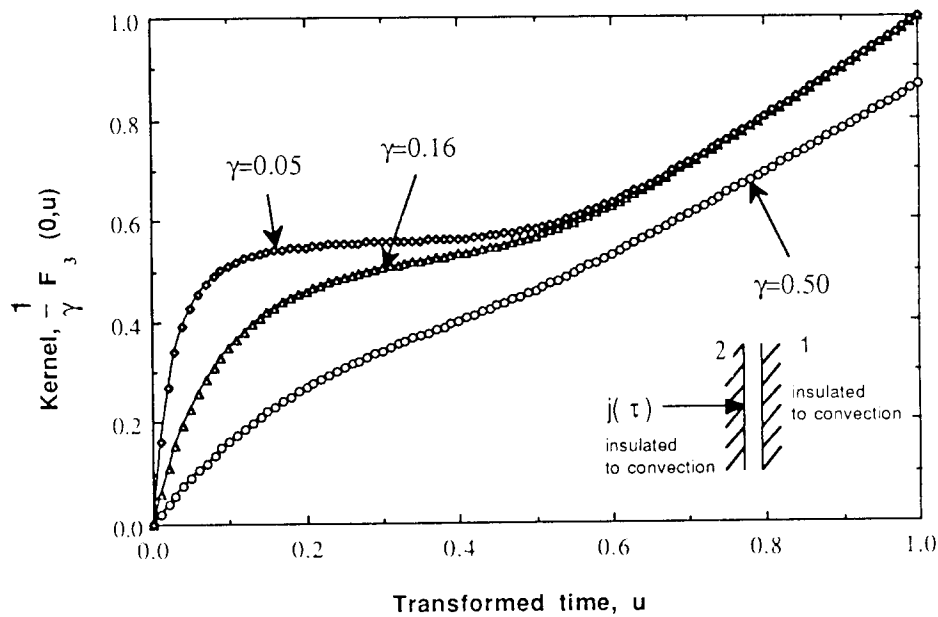


**Fig. 2b.** Variation of  $(1/\gamma)F_3(0, u)$  with  $u$  and  $\gamma$ . The area under this curve from 0 to  $\sqrt{\tau}$  is the temperature of the inner surface for the sample case,  $j = \frac{1}{2}$  and  $\phi_1 = \phi_2 = 0$ . The symbols indicate the numerical data points at fixed  $u$  intervals ( $\Delta u = 0.01$ ).

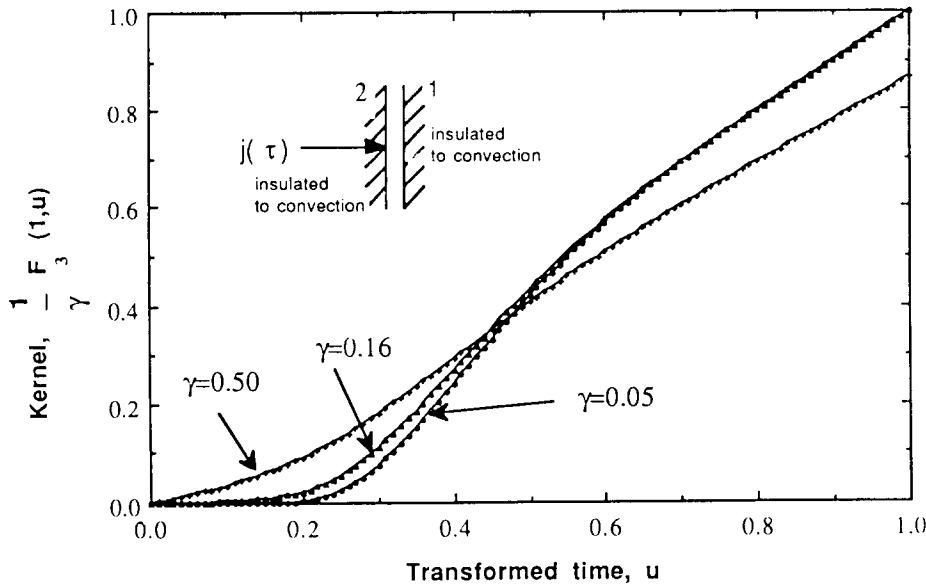


**Fig. 2c.** Variation of  $(1/\gamma)F_3(1, u)$  with  $u$  and  $\gamma$ . The area under this curve from 0 to  $\sqrt{\tau}$  is the temperature of the outer surface for the sample case,  $j = \frac{1}{2}$  and  $\phi_1 = \phi_2 = 0$ . The symbols indicate the numerical data points at fixed  $u$  intervals ( $\Delta u = 0.01$ ).

$\phi_2 = j = 0$ . Since  $\phi_1$  represents heat loss from the outer surface,  $\theta(0, \tau)$  should decrease with time when  $\phi_1 > 0$ . Thus,  $F_1(0, u)$  monotonically decreases with  $u$ . Also, since the initial condition is  $\theta(0, 0) = 0$ , a positive  $\phi_1$  implies that  $\theta(0, \tau)$  should become negative. Therefore,  $F_1(0, u)$  is negative. The magnitude of  $F_1(0, u)$  remains close to 0 till  $u$  approximately reaches 0.4. The reason is that the thermal diffusion wave emerging at the outer surface due to the sudden heat loss at  $\tau = 0$  takes some time to reach the inner surface.

The variation of  $F_2(0, u)$  also shown in Fig. 2a, is analogous to that of  $F_1(0, u)$  for  $\phi_1 = j = 0$  and  $\phi_2 = \frac{1}{2}$  except that now  $\phi_2$  represents heat gain at the inner surface when  $\phi_2 > 0$ . Thus,  $F_2(0, u)$  increases with  $u$  since the area under this curve from  $u = 0$  to  $\sqrt{\tau}$  is equal to the temperature at the inner surface,  $\theta(0, \tau)$ . Also, the temperature of the inner surface instantaneously increases at  $\tau = 0$  when  $\phi_2 > 0$ . Therefore,  $F_2(0, u)$  begins with a positive value. This result can also be obtained by noting that the limit of  $F_2(0, u)$  as  $u \rightarrow 0$  is equal to  $2/\sqrt{\pi}$ . The plots of  $F_1(1, u)$  and  $F_2(1, u)$  are not shown here since  $F_1(1, u) = -F_2(0, u)$  and  $F_2(1, u) = -F_1(0, u)$ .

Figure 2b shows the variation of  $(1/\gamma)F_3(0, u)$  with  $u$  for different values of the dimensionless decay length,  $\gamma$ . As suggested by eqn (12), the area under the curve,  $(1/\gamma)F_3(0, u)$  from  $u = 0$  to  $\sqrt{\tau}$  is equal to

$\theta(0, \tau)$ , the dimensionless temperature of inner surface for  $j = \frac{1}{2}$  with  $\phi_1 = \phi_2 = 0$ . For a constant value of  $\gamma$ ,  $(1/\gamma)F_3(0, u)$  increases with  $u$ , since the imposed radiative flux increases the temperature of the inner surface,  $x = 0$ . At a particular value of  $u$ ,  $(1/\gamma)F_3(0, u)$  decreases as  $\gamma$  increases because a smaller amount of net radiation is absorbed in the glass. In the limit as  $\tau \rightarrow \infty$ , the variation of  $F_3(0, u)$  with respect to  $u$  is linear since the diffusion effects cease.

The variation of  $(1/\gamma)F_3(1, u)$  with  $u$  for different values of  $\gamma$  is shown in Fig. 2c. The area under this curve from  $u = 0$  to  $\sqrt{\tau}$  is equal to  $\theta(1, u)$ , the dimensionless temperature at the outer surface, when  $j = \frac{1}{2}$  and  $\phi_1 = \phi_2 = 0$ . Here again,  $(1/\gamma)F_3(1, u)$  increases with  $u$  because the imposed radiative heat flux increases the temperature of the glass. In the limit as  $\tau \rightarrow \infty$ , the variation of  $F_3(1, u)$  with respect to  $u$  is linear due to no diffusion effects. Figure 2c however, differs significantly from Fig. 2b in the variation with respect to  $\gamma$ . This can be explained as follows. In Fig. 2c, two different time zones,  $u < 0.4$  and  $u > 0.4$  can be identified. The earlier time zone occurs when the thermal diffusion wave emerging at  $x = 0$ , resulting from the temperature difference between the surfaces, has not reached  $x = L$ . In this time zone, the temperature of the outer surface,  $\theta(1, \tau)$ , increases only due to the radiative flux. Therefore, as  $\gamma$  increases, more radiation reaches the outer surface, and  $\theta(1, \tau)$  and  $(1/\gamma)F_3(0, u)$  increase. In the later time zone, the thermal wave emerging at  $x = 0$ , reaches the outer surface  $x = L$ . Here,  $\theta(1, \tau)$  decreases with an increase in  $\gamma$  because a smaller amount of net radiation is absorbed by the glass.

## EXACT SOLUTION

An exact solution to eqn (7) subject to eqns (8)–(10) can be obtained for the case of linearized radiation and constant heat transfer coefficients, ambient temperatures and emissivities on both sides of glass. Here, the radiative heat loss from both surfaces of the glass is linearized giving effective heat transfer coefficients. Therefore, all terms in eqns A(3)–A(9) of the Appendix which contain emissivities are dropped. The technique used to solve this problem is separation of variables. First, the solution is divided into a steady state and a transient part. The steady-state part of the solution is then trivial and the transient part is obtained by solving the resulting eigenvalue problem. The solution is:

$$\theta(\xi, \tau) = u(\xi, \tau) + v(\xi) \quad (20)$$

where:

$$v(\xi) = p\xi + q \quad (21)$$

and:

$$p = -\frac{Bi_1 Bi_2 (\theta_{2\infty} - \theta_{1\infty})}{Bi_1 + Bi_2 + Bi_1 Bi_2} \quad \text{and} \quad q = \frac{Bi_1 \theta_{1\infty} + Bi_2 \theta_{2\infty} + Bi_1 Bi_2 \theta_{2\infty}}{Bi_1 + Bi_2 + Bi_1 Bi_2} \quad (22)$$

The constants  $\theta_{2\infty}$ ,  $\theta_{1\infty}$ ,  $Bi_1$  and  $Bi_2$  are defined as:

$$\theta_{2\infty} = \frac{T_{2\infty} - T_c}{T_c}, \quad \theta_{1\infty} = \frac{T_{1\infty} - T_c}{T_c}, \quad Bi_1 = \frac{h_1 L}{k} \quad \text{and} \quad Bi_2 = \frac{h_2 L}{k} \quad (23)$$

where  $h_1$  and  $h_2$  are the heat transfer coefficients. The solution for  $u(\xi, \tau)$  is given by:

$$u = \sum_{n=0}^{\infty} \left[ C_n e^{-\lambda_n^2 \tau} + \int_0^{\tau} e^{-\lambda_n^2(\tau-\eta)} w_n(\eta) d\eta \right] \phi_n(\xi) \quad (24)$$

where the characteristic functions  $\phi_n$  are:

$$\phi_n(\xi) = \lambda_n \cos(\lambda_n \xi) + Bi_2 \sin(\lambda_n \xi) \quad (25)$$

and the eigenvalues  $\lambda_n$  are obtained from the solutions to:

$$\cot \lambda_n = \frac{\lambda_n^2 - Bi_1 Bi_2}{\lambda_n (Bi_1 + Bi_2)} \quad (26)$$

The constants  $C_n$ , weight functions  $w_n$  and norm  $N(\lambda_n)$  appearing in the equation for  $u(\xi, \tau)$  are defined as:

$$C_n = -\frac{1}{N(\lambda_n)} \int_0^1 v(\xi) \phi_n(\xi) d\xi, \quad w_n(\tau) = \frac{1}{\gamma N(\lambda_n)} \int_0^1 j(\tau) e^{-\xi/\gamma} \phi_n(\xi) d\xi \quad (27)$$

and:

$$N(\lambda_n) = \frac{1}{2} \left[ (\lambda_n^2 + Bi_2^2) \left( 1 + \frac{Bi_1}{\lambda_n^2 + Bi_1^2} \right) + Bi_2 \right] \quad (28)$$

Comparison between exact and numerical solutions showed that, for a dimensionless time step of 0.002, the agreement was within 0.5%. The exact solution, however, cannot be used to simulate real evolving fire environments.

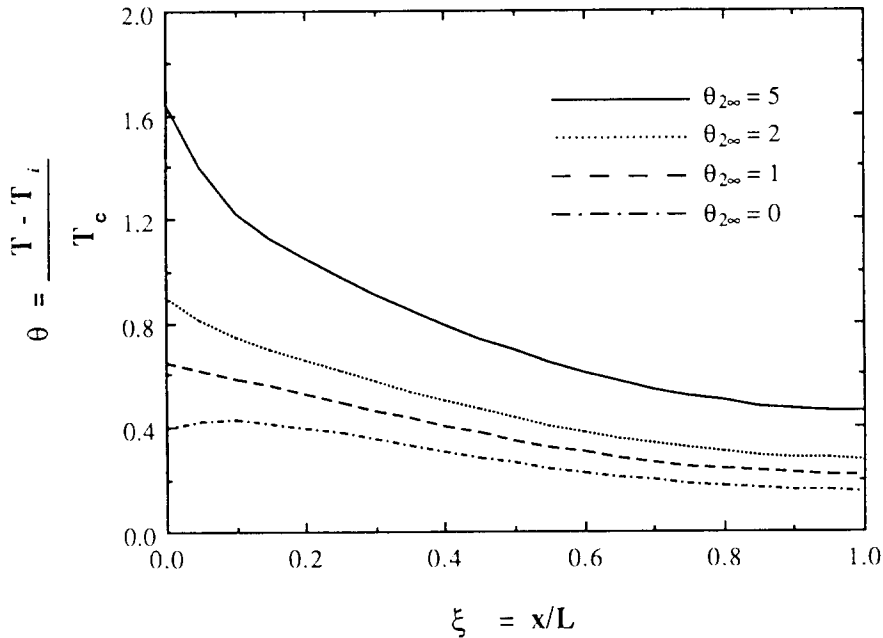


Fig. 3. Temperature profiles as functions of  $\theta_{2x}$ . Here,  $j = 1$ ,  $\tau = 0.3$ ,  $Bi_2 = 0.5$ ,  $Bi_1 = 0.1$  and  $\theta_{1x} = 0$ .

### Profiles

In this section, the temperature profiles obtained in glass using the exact solution are explored as functions of different parameters to estimate the temperature distribution within the glass. Figure 3 shows the temperature profile as a function of the dimensionless hot layer temperature,  $\theta_{2x}$ . Here,  $\theta_{1x} = 0$ ,  $j = 1$ ,  $Bi_1 = 0.1$ ,  $Bi_2 = 0.5$  and  $\tau = 0.3$ . These values are chosen because they are typical of real fires. For example, for a glass window of 5 mm thickness, and thermal conductivity of 0.76 W/m-K,  $Bi_1 = 0.1$  would correspond to  $h_1 = 15.2$  W/m<sup>2</sup>-K which is typical of natural convection in air on the outer surface exposed to ambience. The inner surface heat transfer coefficient would then be equal to 76 W/m<sup>2</sup>-K which is typical of forced convection by the hot fire gases and  $I = 28$  kW/m<sup>2</sup>, which is typical of a compartment fire. For these parameters, the temperature of the glass increases with an increase in  $\theta_{2x}$  due to a larger heat influx. The maximum temperature of the glass occurs at the inner surface as long as the gas temperature remains higher than the glass temperature otherwise it occurs in the interior of the glass since the glass loses heat on both the sides due to convection.

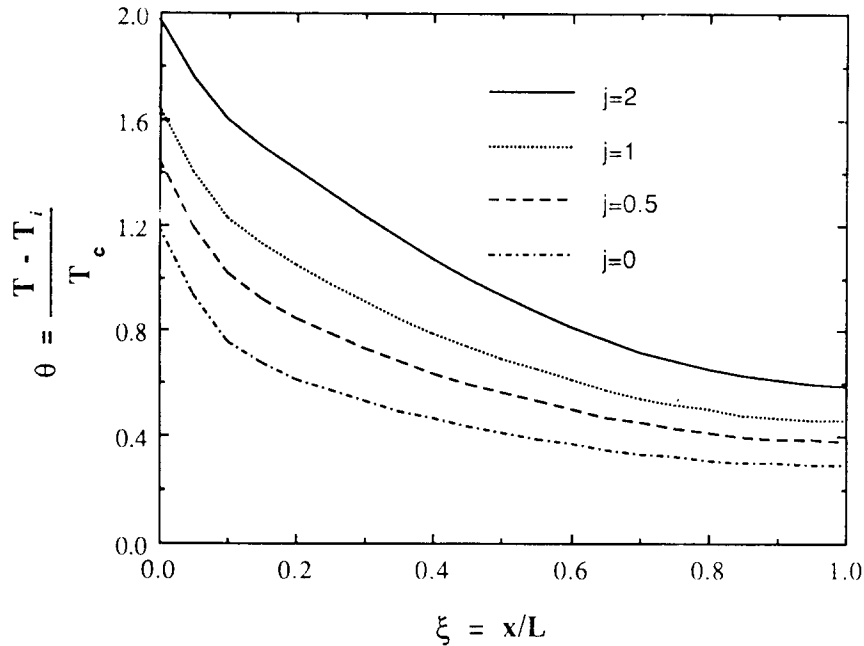


Fig. 4. Temperature profiles as functions of  $j$ . Here,  $\theta_{2x} = 5.0$ ,  $\theta_{1x} = 0$ ,  $Bi_2 = 0.5$ ,  $Bi_1 = 0.1$  and  $\tau = 0.3$ .

Figure 4 shows the temperature profiles as functions of  $j$ . Here  $\theta_{2x} = 5$ ,  $\theta_{1x} = 0$ ,  $\tau = 0.3$ ,  $Bi_2 = 0.5$  and  $Bi_1 = 0.1$ . The temperature increases with an increase in  $j$  as expected. The variation of temperature profiles with  $Bi_2$  showed that the temperature at the inner surface increases with an increase of  $Bi_2$  when  $\theta_{2x} = 5$ . This is a typical value of hot gas temperature in real fires at the time of breakage. In all the cases considered, significant temperature gradients exist within the glass thickness, implying that a uniform glass temperature approximation is not valid in real fire situations.

#### PARAMETERS

Figure 5 shows the temperature history of the inner glass surface, for different values of dimensionless decay length,  $\gamma$ . Biot numbers are held constant and the hot gas temperature was calculated from FIRST<sup>10</sup> for a recent full scale fire.<sup>8</sup> Here  $I = 10 \text{ kW/m}^2$  and represents a window adjacent to the fire. The temperature of the inner surface increases with a decrease in  $\gamma$  because a small value of  $\gamma$  implies that most of the incident radiation is absorbed within a short distance into the glass

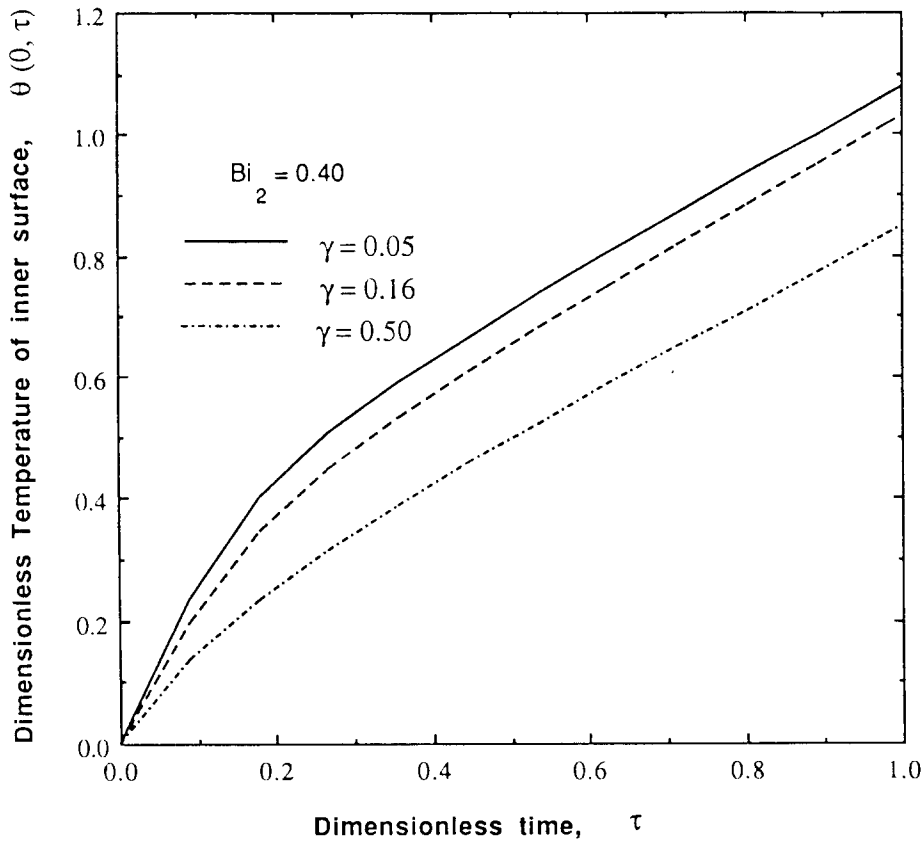


Fig. 5. Dimensionless temperature history of the inner surface as a function of  $\gamma$ . Here,  $Bi_2 = 0.40$ ,  $Bi_1 = 0.04$ ,  $j(\tau) = 1.14$ ,  $T_{1\infty} = T_i = 300$  K and the  $T_{2\infty}$  variation was calculated using FIRST<sup>10</sup> for a recent full-scale fire.<sup>8</sup>

thickness, thus increasing the temperature of the inner surface. For large values of  $\gamma$ , less net radiant flux is absorbed in the glass and the glass behaves more like a transparent medium. A similar calculation was carried out to observe the effect of Biot number  $Bi_2$  on the inner surface temperature. Here,  $I = 0$  and the variation of the hot gas temperature was the same as in Fig. 5. The inner surface temperature increased with an increase in  $Bi_2$  due to a higher heat influx as expected.

The temperature history of the inner glass surface with respect to varying input radiative flux function,  $j(\tau)$  was also explored holding all other parameters constant. The temperature history of the inner surface was seen to roughly follow the integral with respect to time of the incoming radiation.

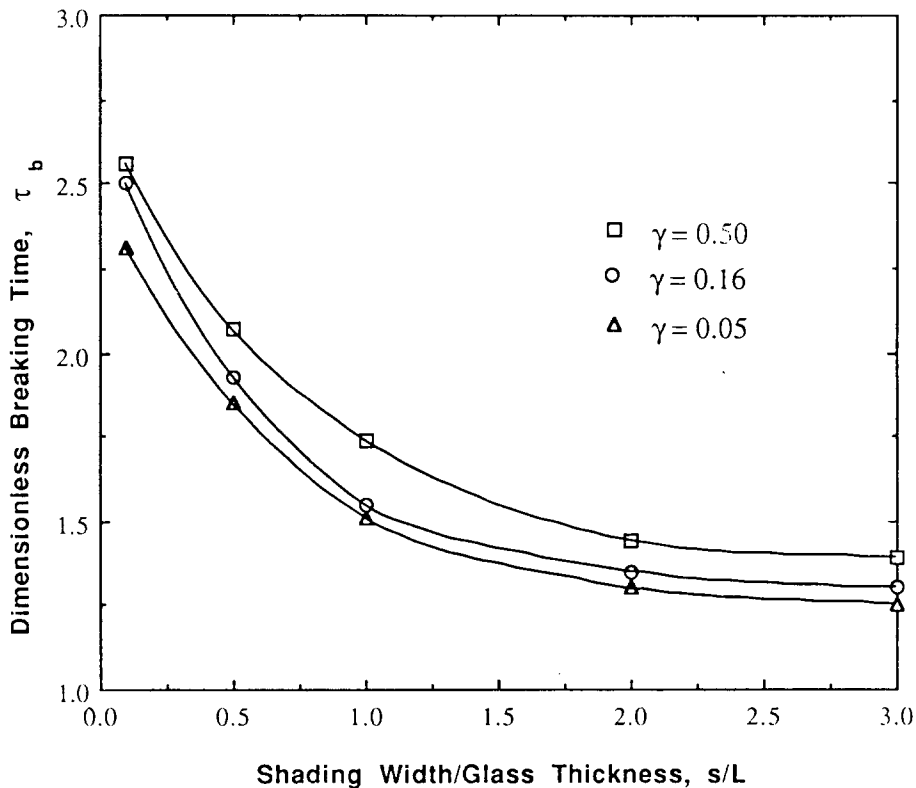


Fig. 6. Variation of the dimensionless breaking time,  $\tau_b$ , with dimensionless shading thickness,  $s/L$ , for different values of absorption length,  $\gamma$ . Here,  $\phi_2 = 1.0$ ,  $\phi_1/\phi_2 = \frac{1}{3}$  and  $j/\phi_2 = 1$ .

### TIME TO BREAKAGE

The time to breakage is defined as the time at which the tensile stress at the shaded edge of the glass reaches the breaking stress. Figure 6 shows the variation of the dimensionless time to breakage as a function of the dimensionless shaded width,  $s/L$ , and the decay length,  $\gamma$ , with  $\phi_1/\phi_2 = 0.33$ ,  $\phi_2 = 0.5$  and  $j/\phi_2 = 1.0$ . The thickness of the window glass is assumed to remain constant. The time to breakage increases with a decrease in shading thickness. The reason is that the tensile stress at the shaded edge is proportional to the difference between the exposed central and the shaded edge temperatures. If the shaded width is small, the edge temperature increases due to thermal diffusion, thus decreasing the tensile stress. Therefore, the central exposed surface temperature must be higher to reach breaking stress and hence the breaking time is longer. The breaking time also increases with an

increase in decay length because more radiation is transmitted through the glass as  $\gamma$  increases.

### ENERGY AND HEAT FLUX MAPS

In this section, the magnitudes of energy and heat flux from various inputs and outputs for the window glass are represented in terms of stacked bar charts. The heat inputs are convection and radiation from the gases,  $Q_c$  and  $q_c$  and  $Q_r$  and  $q_r$  respectively, and radiation from the fire,  $Q_f$  and  $q_f$ . The outputs are defined as heat losses from the outer surface,  $Q_1$  and  $q_1$ , radiative heat loss by emission from the inner surface,  $Q_{2r}$  and  $q_{2r}$ , heat diffusion into the shaded portion of the glass,  $Q_y$  and  $q_y$ , and the rate of energy storage in glass,  $Q_s$  and  $q_s$ . The heat diffusion into the shaded glass was estimated by assuming a hyperbolic tangent temperature profile for the temperature averaged from 0 to  $L$  under the frame.

Figure 7a shows the energy distribution evolution for the case of Fig. 5 where the glass is far away from the fire so that  $j(\tau) = 0$ . The hot gas temperature variation was calculated using FIRST<sup>10</sup> for a recent full-scale fire. Thus, the glass heats up only by convection from hot gases. It is clear that very little heat diffuses into the shaded portion

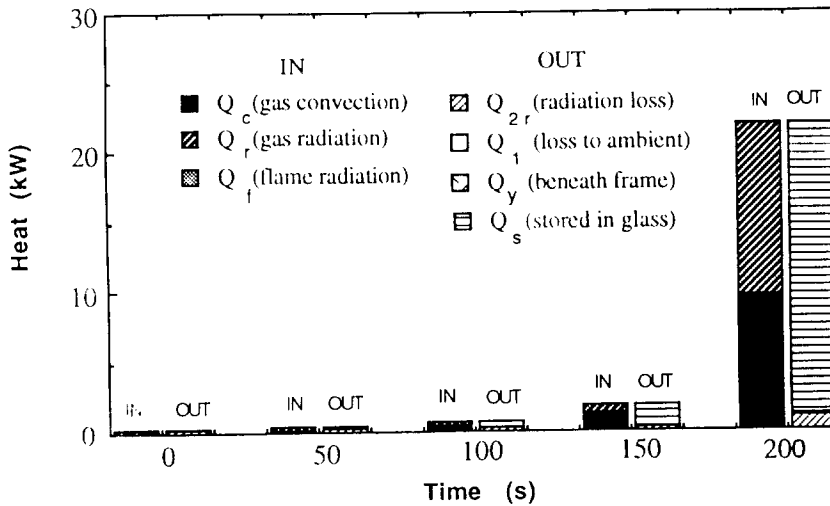


**Fig. 7a.** Energy map representing the different heat sources and sinks for the compartment fire shown in Fig. 2 of Ref. 8. The parameters are the same as in Fig. 5 except here  $j = 0$ .

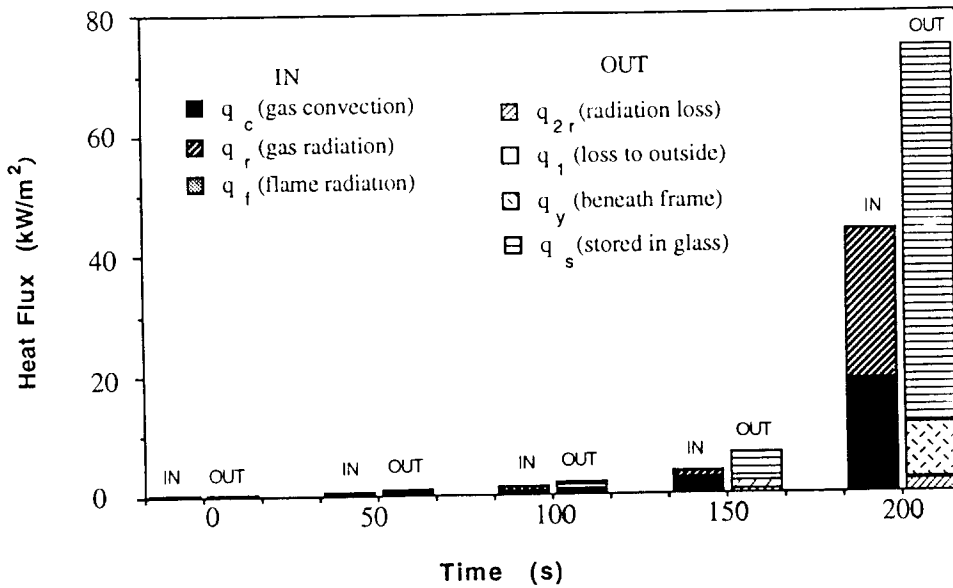


Fig. 7b. Heat flux map representing the different heat sources and sinks for the compartment fire shown in Fig. 2 of Ref. 8. All parameters are the same as in Fig. 5 except here  $j = 0$ .

of the glass. This occurs even though the heat flux is quite substantial (Fig. 7b) due to the very small cross-sectional area of the window glass. The heat loss from the outer side (side 1) is also quite small as the temperature of the outer surface remains near the ambient temperature. The radiative heat loss from side 2 (the inner surface) is the largest loss since the glass temperature is a maximum at the inner surface. Most of the energy is stored in the glass, increasing its temperature. The heat flux distribution evolution is similar to that of the energy distribution with the exception of the heat flow under the frame. The storage heat flux was calculated as the rate of change of internal energy integrated over the glass thickness.

### CONCLUSIONS

The variation of the kernels obtained in the solution of the glass surface temperatures are explored as functions of time and decay length. The magnitudes of all kernels increase with time as the area under the kernels represents the temperature of the glass surfaces. The kernels  $(1/\gamma)F_3(0, u)$  and  $(1/\gamma)F_3(1, u)$ , which represent the temperatures of inner and outer surfaces, respectively, when insulated to convection,

decrease in magnitude as  $\gamma$  increases because a smaller amount of radiation is absorbed in the glass. The dependence of temperature profiles on various parameters is also examined and it is concluded that in a fire environment, a uniform approximation for the glass temperature distribution with depth is not valid due to the presence of large temperature differences between the inner and outer surfaces. The dependence of glass surface temperature histories on various parameters is investigated. The surface temperature increases with a decrease in the decay length,  $\gamma$ . The temperature also increases with an increase in dimensionless heat transfer coefficient on the inner side,  $Bi_2$ , if the hot layer gas temperature is higher than the glass temperature. Also, the inner surface temperature varies roughly as the integral with respect to time of the unsteady radiative flux,  $j(\tau)$ .

The variation of the breaking time of glass windows is determined as a function of decay length,  $\gamma$ , and window geometry,  $s/L$  and  $H/L$ . Breaking time decreases as decay length decreases, since more net radiation is absorbed. A large shading also decreases the breaking time. The magnitude of the energy and heat flux from different sources and sinks is compared in bar charts and it is observed that most of the heat is absorbed within the glass, increasing its temperature. The most significant loss term is radiation from the interior glass surface. The heat diffusing into the shaded edge is quite small because the cross-sectional area of the glass is small. The heat loss from the outer surface is low because the temperature difference between the outer glass surface and the ambience is usually low.

#### ACKNOWLEDGMENTS

The advice of H. R. Baum was crucial to the solution of this problem. Support from the Building and Fire Research Laboratory at the United States National Institute of Standards and Technology under Grant No. 60NANB80848 is very much appreciated.

#### REFERENCES

1. Emmons, H. W., The needed fire science. In *Fire Safety Science—Proc. 1st Int. Symp.*, ed. C. E. Grant & P. J. Pagni. Hemisphere, Washington, DC, 1986, p. 33.
2. Barth, P. K. & Sung, H., Glass Fracture under Intense Heating. Senior course project, Harvard University, Cambridge, MA, 1977.

3. Pagni, P. J., Fire physics—Promises, problems and progress. In *Fire Safety Science—Proc. 2nd Int. Symp.*, ed. T. Wakamatsu *et al.* Hemisphere, Washington, DC, 1988, p. 49.
4. Popov, I., *Introduction to the Mechanics of Solids*. Prentice-Hall, New York, 1979, p. 441.
5. Keski-Rahkonen, O., Breaking of window glass close to fire. *Fire and Materials*, **12** (1988) 61.
6. Keski-Rahkonen, O., Breaking of window glass close to fire II; Circular panes. *Fire and Materials*, **15** (1991) 11.
7. Skelly, M. J., Roby, R. J. & Beyler, C. L., Window breakage in compartment fires. *J. Fire Protection Engg*, **3** (1991) 25.
8. Pagni, P. J. & Joshi, A. A., Glass breaking in fires. In *Fire Safety Science—Proc. 3rd Int. Symp.*, ed. G. Cox & B. Longford. Hemisphere, Washington, DC, 1991, p. 791.
9. Gardon, R., A review of radiant heat transfer in glass. *J. Amer. Ceramic Soc.*, **44** (1961) 305.
10. Mitler, H. E. & Rockett, J. A., User's guide to FIRST, a comprehensive single-room fire model. Report No. 87-3595. National Institute of Standards and Technology, Gaithersburg, MD, 1987, p. 124.

#### APPENDIX: HEAT FLUX EXPRESSIONS

The heat fluxes in eqns (9) and (10) are:

$$\phi_2(\tau) = A + B\theta(0, \tau) + C\theta^2(0, \tau) + D\theta^3(0, \tau) + E\theta^4(0, \tau) \quad (\text{A1})$$

and:

$$\phi_1(\tau) = F + G\theta(1, \tau) - C\theta^2(1, \tau) - D\theta^3(1, \tau) - E\theta^4(1, \tau) \quad (\text{A2})$$

where:

$$A = \frac{h_2 L(T_{2\infty}(t) - T_i)}{kT_c} + \frac{\varepsilon_{2\infty} \sigma L T_{2\infty}^4(t)}{kT_c} - \frac{\varepsilon \sigma L T_i^4}{kT_c} \quad (\text{A3})$$

$$B = -\frac{h_2 L}{k} - \frac{4\varepsilon \sigma T_i^3 L}{k} \quad (\text{A4})$$

$$C = -\frac{6\varepsilon \sigma T_c T_i^2 L}{k} \quad (\text{A5})$$

$$D = -\frac{4\varepsilon \sigma T_c^2 T_i L}{k} \quad (\text{A6})$$

$$E = -\frac{\varepsilon \sigma T_c^3 L}{k} \quad (\text{A7})$$

$$F = \frac{h_1 L(T_i - T_{1\infty}(t))}{kT_c} - \frac{\varepsilon_{1\infty} \sigma T_{1\infty}^4(t) L}{kT_c} + \frac{\varepsilon \sigma L T_i^4}{kT_c} \quad (\text{A8})$$

$$G = \frac{h_1 L}{k} + \frac{4\varepsilon \sigma T_i^3 L}{k} \quad (\text{A9})$$